

Neural networks associated with eye movements in congenital blindness

Cemal Koba¹  | Alessandro Crimi¹  | Olivier Collignon^{2,3}  |
Emiliano Ricciardi⁴  | Uri Hasson⁵ 

¹Computer Vision Team, Sano Centre for Computational Medicine, Krakow, Poland

²University of Louvain (UCLouvain), Institute for Research in Psychology (IPSY) & Neuroscience (IoNS), Louvain, Belgium

³HES-SO Valais-Wallis, The Sense Innovation and Research Center, School of Health Sciences, Lausanne, Sion, Switzerland

⁴MoMiLab, IMT School for Advanced Studies Lucca, Lucca, Italy

⁵Center for Mind/Brain Sciences (CIMEC), The University of Trento, Trento, Italy

Correspondence

Uri Hasson, Center for Mind/Brain Sciences (CIMEC), The University of Trento, Trento, Italy.

Email: uri.hasson@unitn.it

Funding information

Horizon 2020 Framework Programme, Grant/Award Numbers: 857533, MEiN/2023/DIR/379, MEiN/2023/DIR/379; Fundacja na rzecz Nauki Polskiej, Grant/Award Numbers: Research Agendas/Sano, Research Agendas/Sano; Ministero della Salute, Grant/Award Numbers: PNRR - INNOVA, PNRR - INNOVA; Horizon 2020, Grant/Award Number: MEiN/2023/DIR/379; European Union's Horizon 2020; Foundation for Polish Science;

Abstract

Recent studies have shown that during the typical resting-state, echo planar imaging (EPI) time series obtained from the eye orbit area correlate with brain regions associated with oculomotor control and lower-level visual cortex. Here, we asked whether congenitally blind (CB) shows similar patterns, suggesting a hard-wired constraint on connectivity. We find that orbital EPI signals in CB do correlate with activity in the motor cortex, but less so with activity in the visual cortex. However, the temporal patterns of this eye movement-related signal differed strongly between CB and sighted controls. Furthermore, in CB, a few participants showed uncoordinated orbital EPI signals between the two eyes, each correlated with activity in different brain networks. Our findings suggest a retained circuitry between motor cortex and eye movements in blind, but also a moderate reorganization due to the absence of visual input, and the inability of CB to control their eye movements or sense their positions.

KEYWORDS

congenital blindness, eyes, fMRI, sensorimotor, visual

Abbreviations: AAL2, Anatomical Automatic Labelling 2; BIDS, Brain Imaging Data Structure; BOLD, blood oxygen level-dependent; CB, congenitally blind; CSF, cerebrospinal fluid; EO, eye orbit; EO-EPI, EPI signal from the eye orbit; EPI, echo planar imaging; EYE_{raw} , mean raw resting-state signal from the eye regions; EYE_{conv} , mean convolved resting-state signal from the eye regions; FC, functional connectivity; FD, framewise displacement; FEF, frontal eye fields; FWE, family-wise error rate; GM, grey matter; INU, intensity non-uniformity; ROI, region of interest; RS, resting state; SC, sighted controls; SDC, susceptibility distortion correction; SEF, supplementary eye field; SMCtx, sensorimotor cortex; T1w, T1-weighted; TFCE, threshold-free cluster enhancement; WM, white matter; VisCtx, visual cortex.

This is an open access article under the terms of the [Creative Commons Attribution](https://creativecommons.org/licenses/by/4.0/) License, which permits use, distribution and reproduction in any medium, provided the original work is properly cited.

© 2024 The Author(s). *European Journal of Neuroscience* published by Federation of European Neuroscience Societies and John Wiley & Sons Ltd.

European Regional Development Fund;
Italian Health Ministry

Edited by: Guillaume Rousselet

1 | INTRODUCTION

Congenital blindness (CB) causes profound changes in the control of eye movements. This includes slow, irregular oscillations that are sometimes uncoordinated between the two eyes (e.g., Kompf & Piper, 1987; Leigh & Zee, 1980). CB individuals are typically unaware of their spontaneous eye movements, are incapable of sensing eye position and cannot voluntarily initiate saccades in a specific direction. Unlike sighted, CB individuals exhibit slow eye drifts following rapid eye movements and saccades. They also lack a normal vestibulo-ocular reflex, where the eyes typically move in the opposite direction to head movement, which suggests an absence of afferent information from the vestibular to the oculomotor systems (Kompf & Piper, 1987). As such, control and feedback loops related to the oculomotor system are strongly altered when visual input is absent since birth.

Of note, in sighted individuals, endogenously driven oculomotor patterns impact the topography and topology of functional brain networks. Specifically, our group previously characterized the neural correlates associated with spontaneous, non-directed eye movements by extracting EPI signal from the eye orbit (EO-EPI) area (Koba et al., 2021), which has been shown to be related to eye movements (e.g., Beauchamp, 2003; Brodoehl et al., 2016; Keck et al., 2009; Koba et al., 2021; Son et al., 2020). In our prior study, EO-EPI data were used as seed time series in modelling whole-brain resting-state (RS) data. In sighted individuals, spontaneous eye movements were associated with bilateral activity in sensorimotor regions (pre- and post-central gyri and central sulcus, including the frontal eye fields), supplementary motor area and cerebellum. Consistent with these observations, partialling out the variance related to the EO-EPI signal from the RS data reduced connectivity between visual cortex (VisCtx) and sensorimotor cortex (SMCtx), thus confirming that oculomotor-related contributions form an important component of RS network topology. The fact that eye movements are related to VisCtx-SMCtx connectivity is per se non-surprising, since these two areas support visuo-motor processing tasks (e.g., Bernardi et al., 2013; Coiner et al., 2019; Pouget, 2015).

Given both the lack of a lifelong visual input and a physiological oculomotor control since birth, understanding whether the altered spontaneous oculomotor activity in CB affects functional brain networks could provide a

deeper understanding of the principles that determine organized patterns of RS connectivity. Consistency in eye movement-related brain activity across blind participants would be indicated by consistent activation at the group level, signifying an eye movement-dependent yet experience-independent role in mediating RS brain connectivity. A plausible alternative hypothesis is that eye movement-related networks will associate with different connectivity patterns across CB individuals. In this case, the disorganized eye movements in CB would heterogeneously impact sensorimotor-to-visual connectivity depending on the individual (e.g., blindness aetiology) and experience-dependent factors. Beyond these general questions, we were also specifically interested in whether functional connectivity (FC) between the sensorimotor system and visual areas is impacted in blindness.

Prior research presents mixed findings in relation to this question. It has been shown that in fetuses, eye movements correlate with activity in VisCtx and SMCtx, which implies that visual experience is unnecessary for this network to develop (Schöpf et al., 2014). Consistent with this observation, Sen et al. (2022) quantified inter-subject variability associated with FC among different brain areas in both sighted controls (SC) and CB and concluded that there are limited plastic changes in the VisCtx-to-SMCtx connectivity of CB individuals. Notably, although the strength profile of RS connectivity was often more heterogeneous in CB than SC, connectivity between VisCtx and SMCtx showed less variability for individuals who lacked visual input since birth. Thus, although a broader functional reorganization at a whole brain level occurs due to the congenital loss of visual input (e.g., Bock & Fine, 2014; Castaldi et al., 2020; Voss, 2019), the sensorimotor system related to oculomotor activity appears to develop early in life and to be less affected by (the lack of) visual experience-related changes. Conversely, other studies showed that CB individuals show reduced RS-FC between visual and sensorimotor systems, suggesting alterations in the visuomotor circuit related to eye movement. This is one of the most notable differences in connectivity already identified by early studies (Y. Liu et al., 2007) and reviews (Bock & Fine, 2014). However, methodological issues should also be considered. According to Guerreiro et al. (2021), connectivity between visual and motor cortices, in sighted and blind, depends on whether they are scanned with their eyes open or closed. In their study, stronger differences between groups were observed when both groups were

blindfolded than when both were scanned with their eyes open.

In conclusion, finding brain activity correlated with eye movements in CB would suggest that although, for CB individuals, the eyes do not transfer information and cannot be controlled or sensed, there still exists a low-level circuitry that is at least co-activated with systems that produce oculomotor movements. More specifically, finding that eye movements synchronize visual and sensorimotor cortices in CB individuals would provide evidence for an intact circuit that serves no recognizable function or computation and may—in this sense—reflect the presence of ‘non-functional connectivity’ in brain networks. In contrast, if eye movements do not synchronize FC between these regions in CB, this would suggest this specific circuit undergoes neuroplastic changes due to lack of functional purpose and would present an alternative explanation for the weaker connectivity between VisCtx and SMCtx repeatedly documented in prior work.

2 | METHODS

Complete details of the dataset and imaging parameters are given in Pelland et al. (2017), and here, we report only the main details. The entire dataset includes 50 participants who participated in a single 5-min functional MRI run (136 volumes). Participants were instructed to keep their eyes closed, relax and not think about anything in particular. Functional time series were acquired using a 3-T TRIO TIM (Siemens) equipped with a 12-channel head coil. Multislice T2*-weighted fMRI images were obtained with a gradient echo-planar sequence using axial slice orientation; repetition time (TR) 2200 ms; echo time (TE) 30 ms; functional anisotropy (FA) 90°; 35 transverse slices; 3.2-mm slice thickness; 0.8-mm gap; field of view (FoV) 192 × 192 mm²; matrix size 64 × 64 × 35; voxel size 3 × 3 × 3.2 mm³. A structural T1-weighted 3D magnetization prepared rapid gradient echo sequence (voxel size 1 × 1 × 1.2 mm³; matrix size 240 × 256; TR 2300 ms; TE 2.91 ms; TI 900 ms; FoV 256; 160 slices) was also acquired for all participants. All of the procedures were approved by the Research Ethics and Scientific Boards of the Centre for Interdisciplinary Research in Rehabilitation of Greater Montreal and the Quebec Bio-Imaging Network. Experiments were undertaken with the understanding and written consent of each subject.

The study involved 50 participants, comprising 14 congenitally blind individuals (9 males, 5 females, mean age 43.93 ± 11.19 years, 12 right-handed, 2 ambidextrous), 11 who became blind later in life (3 males, 8 females, mean age 52.37 ± 5.29 years, 9 right-handed, 2 left-

handed) and 25 SC (10 males, 15 females, mean age 43.36 ± 13.49 years, 23 right-handed, 2 left-handed). In this study, with few exceptions, we present the data and results for the CB only, since the participants with acquired blindness were outside the scope of this study.

We perform two main types of analyses: the first analysis uses only data from the congenitally blind to describe how data from their eye orbits relate to RS connectivity. The second takes a comparative perspective to evaluate the results found for congenitally blind against two reference datasets. The first is a dataset of SC participants whose data were collected using the same protocol as the congenitally blind. We consider however that blindfolding impacts the oculomotor system in sighted, as it induces a state of slow, uncoordinated eye movements (e.g., Allik et al., 1981). For this reason, we also used previously analysed fMRI data from a RS study of SC where they fixated on a screen centre with open eyes. These data reflect a more valid model of oculomotor function in sighted, but with the caveat that coordinated brain activity may be driven by visual activity related to changes in the fixation-cross's position on the retina.

A full presentation of the fMRI data of the CS group scanned with eyes open is provided in Nilsonne et al. (2016), and the key details are as follows. The study included data from 83 participants. The functional scans consisted of an 8-min eyes-open RS protocol. These data were acquired using echo-planar imaging (EPI) with a FoV of 28.8, slice thickness of 3 mm, no interslice gap, axial orientation, 49 slices covering the whole brain, interleaved acquisition from inferior to superior, TE 30, TR 2.5 s and flip angle 75°. We use these data as a reference for defining a priori ROIs.

2.1 | Data preprocessing

The fMRI data were made available in the Brain Imaging Data Structure (BIDS, Gorgolewski et al., 2016) format. Along with the folder and naming standardization, the first four volumes of functional runs were removed to avoid stabilization artefacts (leaving 132 volumes in total), and the resolution of the functional runs was interpolated to 3 × 3 × 4 mm³. The providers of the data confirmed that no other preprocessing steps were applied during the standardization procedure.

The results reported in this manuscript are based on initial preprocessing that we performed using *fMRIPrep* 20.2.1 (Esteban, Markiewicz, et al., 2018; Esteban, Blair, et al., 2018; RRID:SCR_016216), which is based on *Nipype* 1.5.1 (Gorgolewski et al., 2011; Gorgolewski et al., 2018; RRID:SCR_002502). The preprocessing steps applied by *fMRIPrep* are listed below.

2.1.1 | Anatomical data preprocessing

The T1-weighted (T1w) images were corrected for intensity non-uniformity (INU) with N4BiasFieldCorrection (Tustison et al., 2010), distributed with ANTs 2.3.3 (Avants et al., 2008) (RRID:SCR_004757) and used as T1w reference throughout the workflow. The T1w reference was then skull-stripped with a *Nipype* implementation of the *antsBrainExtraction.sh* workflow (from ANTs), using OASIS30ANTs as the target template. Brain tissue segmentation of cerebrospinal fluid (CSF), white matter (WM) and grey matter (GM) were performed on the brain-extracted T1w using fast (Zhang et al., 2001) (FSL 5.0.9, RRID:SCR_002823). Volume-based spatial normalization to one standard space (*MNI152NLin2009cAsym*) was performed through non-linear registration with *antsRegistration* (ANTs 2.3.3), using brain-extracted versions of both T1w reference and the T1w template. The following template was selected for spatial normalization: *ICBM 152 Nonlinear Asymmetrical template version 2009c* (Fonov et al., 2009, RRID:SCR_008796; TemplateFlow ID: MNI152NLin2009cAsym).

2.1.2 | Functional data preprocessing

The following preprocessing was performed on the RS data of each subject. First, a reference volume and its skull-stripped version were generated using a custom methodology of *fMRIPrep*. Susceptibility distortion correction (SDC) was omitted. The blood oxygen level-dependent (BOLD) reference volume was then co-registered to the T1w reference using *flirt* (Jenkinson & Smith, 2001) with the boundary-based registration (Greve & Fischl, 2009) cost-function. Co-registration was configured with nine degrees of freedom to account for distortions remaining in the BOLD reference. Head-motion parameters with respect to the BOLD reference (transformation matrices, and six corresponding rotation and translation parameters) were estimated before any spatiotemporal filtering, using *mcflirt* (Jenkinson et al., 2002) (FSL 5.0.9). The BOLD time series were resampled onto their original, native space by applying the transforms to correct head motion. These resampled BOLD time series will be called *preprocessed BOLD in the original space*, or just *preprocessed BOLD*. The BOLD time series were then resampled into standard space, generating a *preprocessed BOLD run in MNI152NLin2009cAsym space*. All resamplings can be performed with a *single interpolation step* by composing all the pertinent transformations (i.e., head-motion transform matrices, SDC

when available and co-registrations to anatomical and output spaces). Gridded (volumetric) resamplings were performed using *antsApplyTransforms* (ANTs), configured with Lanczos interpolation to minimize the smoothing effects of other kernels (Lanczos, 1964).

Several confounding time series were calculated based on the preprocessed BOLD: framewise displacement (FD) and three region-wise global signals. FD was computed using two formulations following Power et al. (absolute sum of relative motions, Power et al., 2014) and Jenkinson et al., 2002 (relative root mean square displacement between affines, Jenkinson et al., 2002). FD is calculated for each functional run, both using their implementations in *Nipype* following the definitions by Power et al. (2014). The three global signals are extracted within the CSF, the WM and the whole-brain masks.

Many internal operations of *fMRIPrep* use *Nilearn* 0.6.2, RRID:SCR_001362 (Abraham et al., 2014), mostly within the functional processing workflow. For more pipeline details, see the section corresponding to workflows in *fMRIPrep*'s documentation.

After the above procedure applied by *fMRIPrep*, we applied band-pass filtering (0.01–0.1 Hz) and cleaned the data from six main motion parameters, mean WM and CSF signals and FD using *AFNI*'s *3dDeconvolve* (Cox, 1996). The resulting dataset was smoothed with a 6-mm full-width half-maximum (FWHM) kernel with the *3dBlurToFWHM* function of the same software. These smoothed residuals were considered as the RS data to be used in all subsequent analyses.

All the figures in this paper were generated using *Nilearn* (Abraham et al., 2014), *MATLAB version 9.10.0.1613233 (R2021a)* (2021) or *BrainNet Viewer* (Xia et al., 2013).

2.1.3 | Creating the eye orbit EPI (EO-EPI) regressors

The eye orbit (EO) area was marked using *MRICRON* (Rorden et al., 2007) on a common anatomical template *MNI152 NLin 2009c Asym* (Figure S1). The EO region of interest (ROI) covered the entire eye orbit. The mask was drawn on the MNI template and then applied to all participants regardless of their eye vitreous size or availability. The resulting binary ROI mask was resampled to the resolution of the functional runs, and no further processing was needed because all the RS data were already aligned to this common space. The resampled mask was used to extract the mean RS signal from the eye regions (denoted as EYE_{raw}) for each participant.

We expected that the EO-EPI time series extracted from both eyes should be strongly correlated. As reported in Section 3, this was indeed the case for the SC who participated in the current study with their eyes blindfolded. Although for some CB participants, the correlations were low, we still decided to average the time series in such cases. Our motivation was that averaging emphasizes epochs of coordinated movement.

The average time series were also convolved with a basis HRF function using *AFNI*'s *waver* command, producing EYE_{conv} . We convolved the EO-EPI signal because in our previous research (Koba et al., 2021), we investigated the temporal dynamics between EO-EPI data and eye tracking measurements and documented a tight correspondence between EO-EPI peaks and peaks in eye velocity changes. Specifically, EO-EPI data lagged the eye tracking data by approximately 2 s, in a study with an EPI repetition time of 2.5 s. This suggests that the EO-EPI fluctuations do not represent BOLD signal per se (and, for this reason, do not reflect HRF-driven smoothing), but rather fluctuations in the EPI contrast due to shifts in the location of the vitreous humour and optic nerve (for supporting data, see Keck et al., 2009). For completeness, in separate analyses, we used either EYE_{raw} or EYE_{conv} as 'seed' regressors to identify brain areas correlated with the EO-EPI signal.

Finally, in a few cases, we documented highly divergent EO-EPI time series profiles between the two eyes. As exploratory analyses, in the most marked cases, we produced whole-brain FC networks from the time series of each eye separately.

2.2 | Statistical inference of fMRI analyses

2.2.1 | Correlates of EO-EPI regressors

We conducted a whole-brain single-voxel regression for each participant using a univariate linear model. In this model, EYE_{raw} was the predictor variable and voxel-wise RS data was the outcome variable (note that nuisance factors were removed during preprocessing). The significance of the beta coefficients was determined at the group level using *FSL*'s *randomize* function (Winkler et al., 2014). This function applies a one-sample *T*-test and determines the significance threshold through 10,000 permutations and threshold-free cluster enhancement (TFCE). The age and sex of each subject were accounted for in the group-level statistics by inserting them as regressors of no interest. The same procedure was repeated using EYE_{conv} as the seed time series.

To study the relationship between EO-EPI activity and regions previously associated with oculomotor control, we defined functional regions whose activity has been linked to eye movements. These include the frontal eye fields (FEF), supplementary eye field (SEF), intraparietal sulcus, middle occipital gyrus, V5/mT, V1 and vermis of the cerebellum. We defined these regions by using the NeuroSynth database (Yarkoni et al., 2011). Specifically, we used a probability mask corresponding to the keyword *eye* and applied a z-score threshold of $Z = 4$ generated from 417 studies. The thresholded image was then clustered with a voxel threshold of 30. The resulting binarized image produced the separate functional ROIs used in this analysis (Figure S3). They were used as independent ROIs for computing the significance of EO-EPI coefficients via a Wilcoxon rank sum test, in each region.

2.2.2 | The impact of eye movement on connectivity

To create FC networks, we used a RS FC parcellation based on 400 ROIs grouped by seven networks: Visual, Somatomotor, Dorsal Attention, Ventral Attention, Limbic, Frontoparietal and Default Mode (Glen et al., 2021; Schaefer et al., 2018). This parcellation was also aligned to the template we used (MNI152NLin2009cAsym). We extracted the mean time-series from each ROI, for the two types of spatially smoothed RS data we derived (one typical, and the other with EO-EPI EYE_{raw} regressed out).

To determine the effect of partialling out EYE_{raw} from the RS data on FC networks, as a first step, we constructed two variants of the 400×400 connectivity matrix. Each was created by correlating the mean RS time series extracted from the 400 ROIs using the Schaefer et al. (2018) atlas. One matrix was based on the original RS data, and the other used the RS data that was cleaned of EYE_{raw} , that is, where the contribution of variance related to eye movements was removed. Ultimately, this produced two correlation matrices for each participant.

Following the workflow in our prior work (Koba et al., 2021), we examined the network features after thresholding the connectivity matrices at three sparsity levels: 30%, 20% and 10%. From each participant's RS network, the following metrics were derived: node degree, strength, cluster coefficient, transitivity, assortativity, efficiency, number of communities, betweenness centrality and modularity. After thresholding, the feature values were processed as follows. We generally used non-binarized connections maintaining the original weights, with the following exceptions: (a) for node degree we

used binarized values; (b) for clustering coefficient, transitivity and betweenness centrality, we used normalized values, per participant, per condition; (c) for betweenness centrality, we used connection-length matrices as inputs. We calculated these metrics using the Brain Connectivity Toolbox (Rubinov & Sporns, 2010), for both the original and 'clean' networks as defined above. We then tested which of these parameters differed as a result of the EYE_{raw} removal procedure using paired-sample T -tests.

To identify if there were clusters of regions whose connectivity changed after the removal of the EO-EPI data, the two 400×400 connectivity matrices were compared using a difference-network analysis using the Network-Based Statistics Toolbox (NBS, Zalesky et al., 2010), implemented in MATLAB (MATLAB version 9.10.0.1613233 (R2021a), 2021). This analysis quantifies the likelihood of finding a cluster of nodes all of which are more weakly connected in one condition than the other. Initial thresholding (a hyper-parameter) ensures that only strong connections are considered. We used primary t -thresholds of 7.5 and 5.0, 10,000 permutations and an alpha value of 0.05. The same analysis was repeated between the network of SC and CB groups in order to replicate the previous literature.

2.2.3 | Effective connectivity

To further examine the relationship between visual and somatosensory cortex, we used an effective connectivity model based on Granger Causality. The goal was to understand the causal interaction between eye movements, cortical signals and the direction of the connection between the occipital and sensorimotor cortices. The analysis was applied via a custom script written in Python (Van Rossum & Drake, 2009), using the *statsmodels* library (Seabold & Perktold, 2010). Before performing the analysis for effective connectivity, a preliminary step was applied to ensure the stationarity of the time series. More specifically, the augmented Dickey–Fuller test was employed (Dickey & Fuller, 1979). Once the stationarity of the signal was confirmed, we implemented pairwise Granger causality models with an inclusive range of time lag from 1 to 5. The multivariate approach was not used given the small number of regions of interest. After estimating the autoregressive model, F -statistics were computed and converted into p -values. For each subject, each time lag (from 1 to 5 TR) and each causality test (visual-sensorimotor, visual- EYE_{raw} ; sensorimotor- EYE_{raw} , sensorimotor-visual; EYE_{raw} -visual, EYE_{raw} -sensorimotor), p -values were calculated. To avoid sensitivity to outliers, the median across the entire dataset was computed and reported (following Duggento et al., 2018).

3 | RESULTS

3.1 | Temporal characteristics of EO-EPI time series in blind

As expected, CB presented ocular movements with different characteristics than those of SC. In the current dataset, this was evident in several ways. First, we computed the frequency characteristics of the EO-EPI EYE_{raw} time series in CB and compared those with data from blindfolded SC participants whose data were provided in the same dataset. Example time series from CB and SC are presented in Figure 1a. Visual inspection suggests that in CB, the spectral power is more uniformly divided over the frequency range. Higher power was found for CB in both the lower (<0.01 Hz) and higher (0.05–0.1 Hz) frequencies (Figure 1c). EO-EPI data of CB also tended to have a larger variance per time series ($N = 14$, mean = 0.04 ± 0.01), as compared with that of SC ($N = 25$, mean = 0.03 ± 0.001 , $t(37) = 3.15$, $p = 0.003$, Figure 1b). We found similar results when analysing the SC group data that we used in our previous study (Koba et al., 2021), based on the SleepyBrain dataset (Nilsson et al., 2016). These sighted participants also showed lower variance than CB, (SC $N = 82$, mean = 0.03 ± 0.01 , $t(94) = 3.79$, $p < 0.001$, see Figure S2)

As shown in the Supporting Information, for blindfolded SC, EO-EPI time series from each eye were positively correlated. However, this pattern was weaker for CB (Figure S6). In some cases, CB participants had one eye with more pronounced dynamics than the other (Figure S5).

3.2 | Correlates of EO-EPI regressor

Correlates of EYE_{conv} and EYE_{raw} on the whole-brain level were determined via a one-sample T -test whose sampling distribution was determined using 10,000 permutations, and the results were corrected with a family-wise error rate (FWE) of $\alpha = 0.05$ using TFCE. In general, the analysis of the raw signal was more sensitive, identifying a set of clusters consisting of 9048 voxels (3321 positive; 5727 negative), compared with only 4004 voxels found when analysing the convolved signal (64 positive, 3940 negative). Brain regions whose activity covaried with EYE_{raw} are shown in Figure 2. Although a positive relationship is found with bilateral superior frontal sulci, posterior cingulate, lateral occipital cortices and cerebellum, a negative relationship is evident for the sensorimotor cortex. Correlates of EYE_{conv} captured a different, more limited pattern (Figure S4), showing a positive relationship in the head of the right caudate nucleus and a

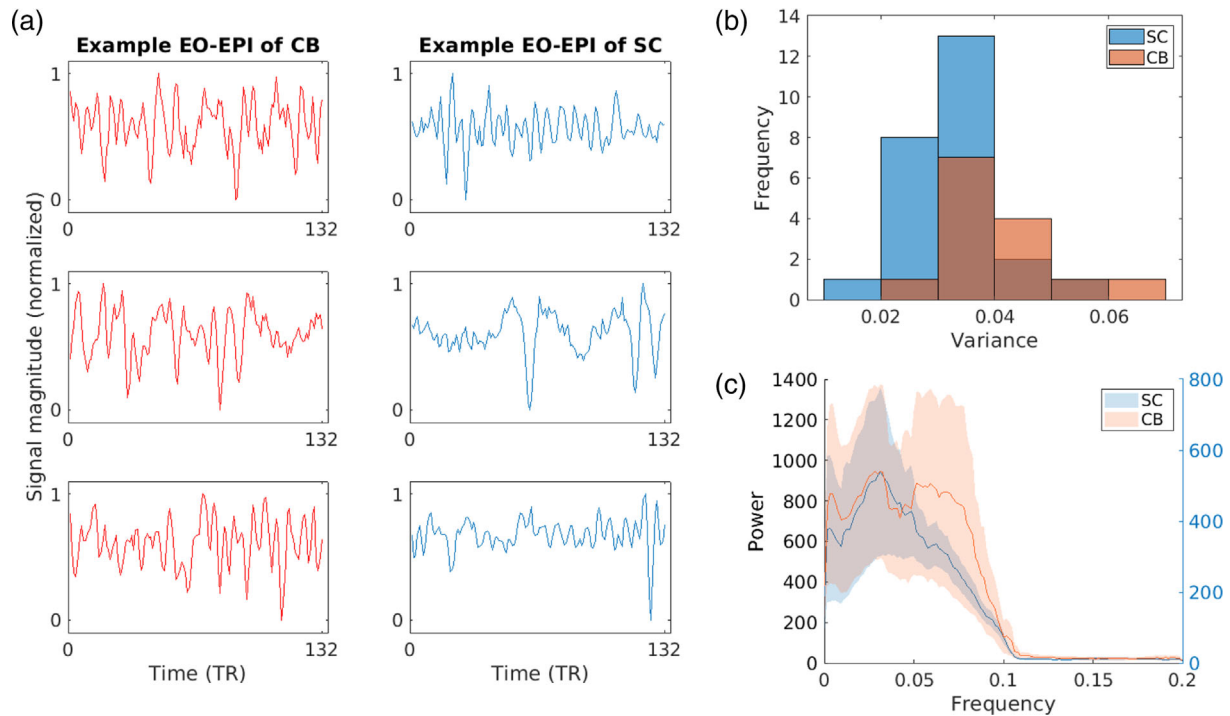


FIGURE 1 Comparison of EO-EPI time series in CB and blindfolded SC. Series from both groups were normalized in the range of 0 to 1. (a) Example EO-EPI time series from CB (left column) and SC (right column). (b) Histogram of the variances of EO-EPI time series. (c) Power-frequency distribution of EO-EPI time series (in Hz).

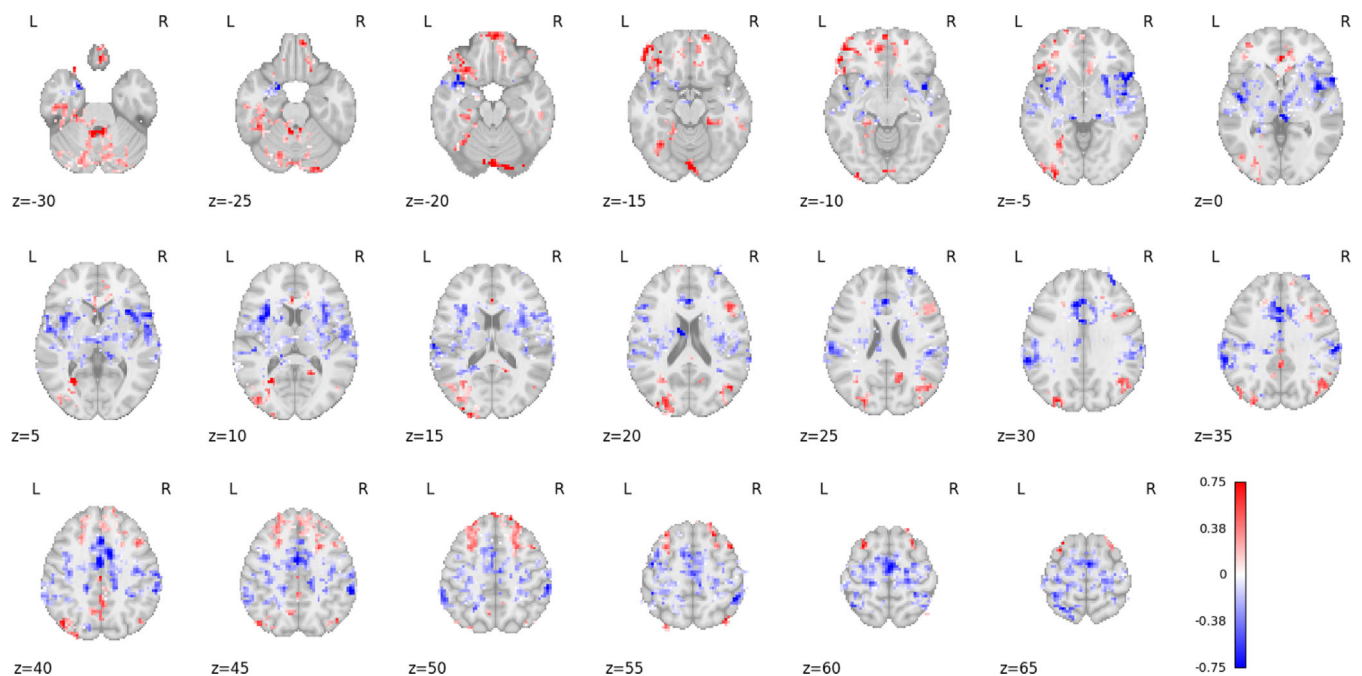


FIGURE 2 Brain areas where BOLD activity correlated with eye movements in congenitally blind. The figure shows correlates of EYErAw, $p < 0.05$, TFCE-corrected for multiple comparisons. The colour bar shows the coefficients of the EYErAw. Warm colours represent positive coefficients; cold colours represent negative ones.

negative relationship for the thalamus and visual cortex. A complete listing of these regions according to the Anatomical Automatic Labelling 2 template (AAL2, Rolls

et al., 2015), Desikan–Killiany (Desikan et al., 2006) and Harvard–Oxford (RRID:SCR_001476) atlases is reported in Tables S1 and S5. In order to investigate the large

clusters in the sensorimotor area and cerebellum, we studied those regions with more specific atlases. For the sensorimotor area, we quantified the distribution of the significant voxels in Brodmann areas 1–6 (atlas file extracted from MRIcro's library (Rorden & Brett, 2000). 57.34% of the significant voxels in those areas were concentrated in area 6 (premotor and supplementary motor cortex), 17.56% were concentrated in area 4 (primary motor cortex–precentral gyrus), and 14.47% in area 3 (primary somatosensory cortex–postcentral gyrus). To investigate the results found in the cerebellum, an anatomical (Diedrichsen et al., 2009) and a functional (King et al., 2019) parcellation were used, both of them available in Diedrichsen and Zhi (2022). The anatomical parcellation suggests that 20.4% of the significant voxels were in Right VI, 17% of them in Vermis-Crus I, 10% in Left Crus II and 9.19% in Right Crus II. The functional parcellation, which divides the cerebellum based on 30 tasks, shows that 37.38% of the voxels belong to the regions related to word comprehension-language processing-narrative tasks (bilaterally), 11.28% are related to divided attention-active maintenance tasks and 10.77% are related to autobiographical recall-interference resolution and visual letter recognition. When restricted to the regions identified as eye-related in a NeuroSynth search (see Section 2) via the Wilcoxon rank sum test, none of the ROIs showed a departure from zero for CB (Table S4).

We compared the spatial distribution of the identified clusters to that found in our previous study (Koba et al., 2021), which included 83 participants. The spatial distribution of activity identified for EYE_{raw} showed higher spatial overlap than that observed for EYE_{conv} , as evidenced by Dice coefficients of 0.25 and 0.09, respectively. For this reason, we proceed with the EYE_{raw} in subsequent analyses. Figure 3 presents the spatial overlap between the statistical maps produced for CB in the current study and sighted individuals in Koba et al. (2021).

As indicated in Section 2, although we averaged the two EO-EPI time series per participant to identify time points of coordinated eye movements, we observed low correlation for some CB participants (five participants showing absolute correlation values below 0.25). For this reason, for two CB participants, we conducted an analysis where connectivity maps were computed separately for each eye. As shown in Figure 4, when the correlation was low, each eye appeared to correlate with activity in different brain networks.

We note that an analysis of RS correlates of EO-EPI of the 14 blindfolded SC controls whose data were collected in the current study did not replicate our prior findings (Koba et al., 2021), which we also replicated for two large independent datasets (Shehzad et al., 2009; van der Meer et al., 2016). Specifically, for these blindfolded SC, we identified no cluster where activity reliably correlated with the EO-EPI regressor. This could be due to the

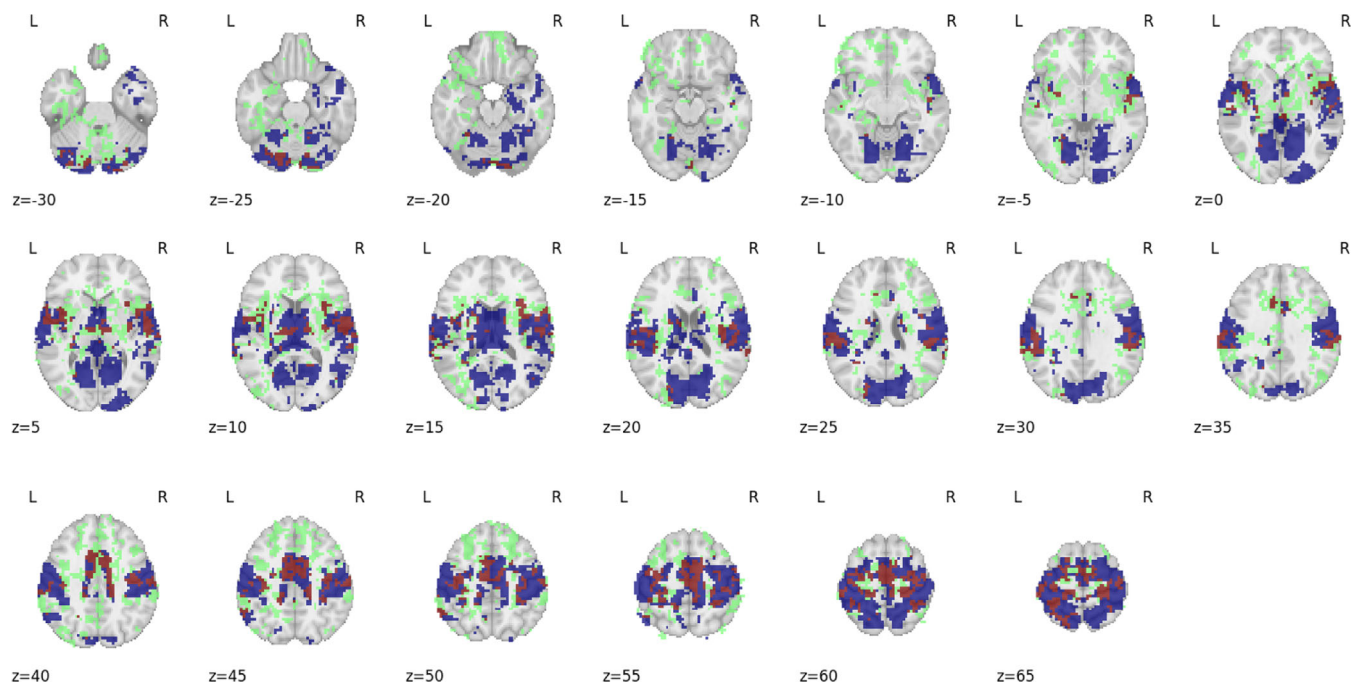


FIGURE 3 Overlap between brain areas correlating with eye movements in congenitally blind in the current study and sighted-controls (SC). Data from SC were collected by Koba et al. (2021). Red areas indicate areas correlated with eye movements for both groups. Blue areas were identified for SC alone ($N = 83$), and green areas for blind alone ($N = 14$). As evident in the figure, both groups show bilateral eye movement-related activity in the sensorimotor cortex and visual cortices.

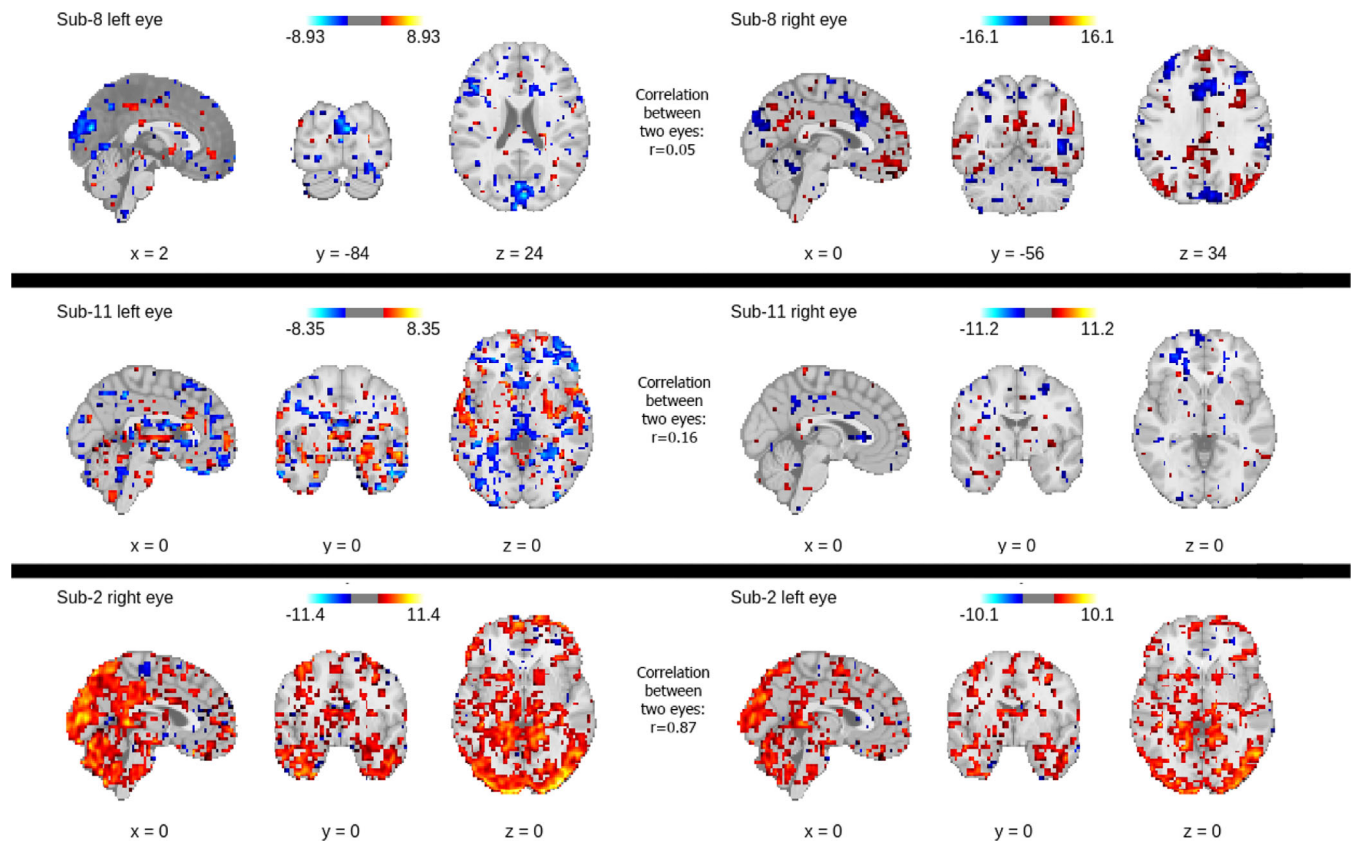


FIGURE 4 Relationship between right or left EO-EPI and RS for sample participants. The first two rows present participants (Sub-8 and Sub-11) whose eyes demonstrate low EO-EPI correlation, and the bottom row (Sub-2) presents a participant with a more typical, high correlation. Images are thresholded at an arbitrary threshold of $T = 2.6$. It can be seen that the right and left eyes correlate with similar regions when the correlation between eyes is high, but with different regions when the correlation between eyes is low.

use of blindfolding in the current study, the small group size or scanning parameters. However, when examining the data patterns for this group at a lower threshold (single voxel p -value of 0.3), it appears that they present similar patterns to those of the CB (Dice coefficient = 0.6). Therefore, we used the regions identified for CB (Figure 2) to investigate the activity in SC in more detail. When restricted to the regions identified by CB, the SC-blindfolded group showed a significant relationship between RS activity and EYE_{raw} in five of the seven clusters (see Table S2).

In addition, we conducted another sensitivity analysis that allowed us to compare the coefficients of eyes open and closed (blindfolded) conditions for sighted participants. For this analysis, we defined functional ROIs from clusters identified by Koba et al. (2021) for sighted individuals scanned with eyes open and then quantified the activation strength (correlation with EO-EPI) within each ROI for blindfolded SC. The data indicate that for three of the eight clusters, the mean correlation computed for blindfolded SC data in the current study was significantly positive (see Table S3). The largest cluster (right cingulate cortex), which included the motor cortex, showed the

most robust result in both the current study and the prior study. The results suggest the whole-brain analysis for blindfolded SC suffers from reduced sensitivity due to a limited number of participants.

3.2.1 | Functional connectivity and derived network metrics

As detailed in Section 2, to evaluate the impact of EO-EPI on FC networks, we created two correlation matrices for each participant, which were derived from the regular RS data and EO-EPI-removed RS data, respectively. To evaluate larger-scale topographical differences in connectivity, we used the Network-Based Statistics (NBS) toolbox to identify difference networks consisting of a continuous set of interconnected edges with lower values in one condition than another. For the EO-EPI-removed networks, there was no significant network difference in CB after the removal of EO-EPI, regardless of the primary threshold used. This suggests that for CB, removal of eye-related activity does not strongly change inter-regional connectivity. As a validity check, we compared the

networks of SC and CB participants in the current study, using data before the removal of the EO-EPI signal. This analysis revealed the expected difference network with decreased connectivity for CB, and the strongest difference holding being between VisCtx and SMCtx (MNI coordinates are 24, -99, 7, and 22, -35, 71, respectively, Figure S7).

We examined the impact of removing the contribution of EO-EPI on several whole-brain global network metrics. In general, the pattern of results was qualitatively similar to what we had found for sighted participants in Koba et al. (2021), with the removal of EO-EPI variance resulting in reduced degree strength and weaker clustering. However, with two exceptions, none of these differences were statistically significant (Table 1). This is likely due to the reduced power in the current study ($N = 14$) as compared with our prior study with sighted participants ($N = 83$). To determine this, we randomly sampled groups of $N = 14$ from our prior study of sighted individuals and analysed the data similarly (100 permutations). For this sample size, no effect was consistently statistically significant for the sighted as well. Still, the most consistent effect in this small-sample simulation was found for the Max Strength parameter where 39% of the permutations were significant at $\text{sparsity} = 0.1$. Importantly, this was one of the two parameters that we

identified for CB as well, for $\text{sparsity} = 0.2$, the other being Max Betweenness Centrality for $\text{sparsity} = 0.3$ (see Table 1). To summarize, our results are consistent with our prior findings for sighted, indicating that the removal of eye movement-related activity impacts the maximal connectivity strength in RS connectivity.

3.2.2 | Effective connectivity

The Granger causality analysis of the three selected ROIs from (i) VisCtx, (ii) SMCtx and (iii) EYErw revealed significant causality from EYErw to the VisCtx (mean p -value across participants; $p = 0.03$) and from the VisCtx to the SMCtx (mean $p = 0.02$). All other tests [SMCtx to EYErw ($p = 0.13$), SMCtx to VisCtx ($p = 0.17$), VisCtx to EYErw ($p = 0.2$) and EYErw to SMCtx ($p = 0.13$)] showed p -values greater than 0.05 (see Figure S8).

4 | DISCUSSION

Here, we present the first study of whether spontaneous eye movements in CB individuals correlate with brain activity. A priori, there are many reasons to question whether congenitally blind should at all show brain

TABLE 1 Difference of network metrics between raw and clean (EO-EPI-removed) functional connectivity matrices.

	Sparsity = 0.1			Sparsity = 0.2			Sparsity = 0.3		
	<i>P</i> -value	<i>T</i> -stat	Effect size	<i>P</i> -value	<i>T</i> -stat	Effect size	<i>P</i> -value	<i>T</i> -stat	Effect size
Max degree	0.15	1.53	0.19	0.06	2.05	0.16	0.97	0.04	0
Min degree	0.34	1.00	0.12	0.46	-0.76	0.07	0.19	-1.39	0.09
Max strength	0.17	1.46	0.14	0.04*	2.31	0.16	0.27	1.16	0.06
Min strength	0.43	0.82	0.11	0.57	-0.59	0.05	0.29	-1.11	0.08
Mean strength	0.15	1.51	0.08	0.12	1.66	0.08	0.11	1.71	0.08
Max cluster coefficient	0.10	1.75	0.15	0.60	0.54	0.02	0.14	1.56	0.08
Min cluster coefficient	0.64	-0.48	0.18	0.48	0.72	0.14	0.15	-1.54	0.17
Mean cluster coefficient	0.12	1.65	0.08	0.12	1.65	0.08	0.10	1.76	0.08
Transitivity	0.17	1.45	0.1	0.19	1.37	0.08	0.14	1.58	0.07
Assortativity	0.27	1.14	0.2	0.32	1.03	0.24	0.34	0.99	0.22
Efficiency	0.24	1.23	0.06	0.11	1.71	0.07	0.12	1.65	0.07
Max number of community	1.00	0.00	0	0.17	-1.44	0.49	0.34	-1.00	0.23
Maximized modularity	0.35	-0.97	0.07	0.65	0.47	0.02	0.60	0.54	0.03
Max betweenness centrality	0.91	0.12	0.01	0.24	1.23	0.07	0.03*	2.49	0.15
Mean betweenness centrality	0.06	2.03	0.17	0.11	1.70	0.08	0.11	1.70	0.08

Note: The p -value in bold font and asterisk denotes the significant differences between regular and clean RS networks.

connectivity that correlates with eye movement: they lack a vestibulo-ocular reflex, cannot initiate voluntary saccades and often display non-coordinated eye movements. Furthermore, even if eye movements were coordinated with brain activity at the individual level, it is still completely conceivable that this organization could result from unconstrained neuroplastic changes, which would produce idiosyncratic reorganization at the individual level, with no consistency at the group level. Contradicting both possibilities, we document robustly systematic patterns of brain activity correlated with eye movements across congenitally blind individuals. The EO-EPI signal was used as a proxy for eye movements (following, e.g., Beauchamp, 2003; Frey et al., 2021; Keck et al., 2009; Koba et al., 2021; Schöpf et al., 2014; Son et al., 2020). Consistent with prior reports (e.g., Kompf & Piper, 1987; Leigh & Zee, 1980), we found strong differences between oculomotor dynamics in CB and SC, with CB showing greater variance in the time series overall (Figure 1b) and increased power in both the higher and lower frequency ranges. A few time series exhibited highly regular oscillatory dynamics (Figure 1a), and some CB participants showed uncorrelated eye movements.

At the group level, we identified brain activity that correlated with the EO-EPI data, for both the raw and convolved versions. As indicated by the Dice coefficient, the distribution of this activity overlapped more strongly with that of SC when using the raw regressor. We note that given the dynamics of CB's EO-EPI time series, the raw time series could correlate with brain activity if peaks in the eye movement follow movement onsets by a 2- to 6-s delay, which is consistent with the slow oscillatory dynamics evident in Figure 1a. EO-EPI signal was correlated with brain activity in regions including the cerebellum, sensorimotor areas bilaterally, supplementary motor area, basal ganglia and thalamus. One difference between the correlates of EO-EPI for CB and those we previously identified for SC was that the non-convolved EO-EPI regressor showed a stronger correlation than the convolved for CB, whereas the correlation pattern was the opposite for SC.

The fact that EO-EPI is correlated with overlapping brain areas in CB and SC (both for eyes-open condition, quantified from Koba et al., 2021, and eyes-closed blindfolded condition) indicates that eye movements may be associated with RS activity, regardless of visual input and visual experience. It is known that visually driven stimulation of the visual system in the first 2 years of life is required for the normal maturation of the visual pathway and its integration with the rest of the brain (reviewed in Fine and Park, 2018, and Voss, 2019). Congenital visual deprivation and sight-recovery studies report that in the absence of early post-natal visual experience, the visual

system shows irreversible functional and structural changes such as increased cortical thickness and cross-modal responses in the primary visual cortex (Collignon et al., 2015; Guerreiro et al., 2015; Hölig et al., 2022; Saenz et al., 2008).

Our findings offer a complementary perspective as the presence of eye movement-related cortical activity in blind individuals may suggest the existence of a purely physiological constraint on connectivity, which reflects an initial, non-pruned state rather than one shaped by perceptual input. This is consistent with the findings of Schöpf et al. (2014), who observed correlations between EO-EPI and RS data in pre-natal infants. An alternative possibility, which is mutually compatible with the previous, is that the neural areas involved in the movement of the oculomotor muscles undergo neuroplastic changes in the blind and become incorporated into different networks so that certain computations and mental processes produce associated eye movements. This could explain why for some CB, different brain networks were associated with the eye movements of the left and right eyes. Interestingly, even in normally sighted, the processing performed by each eye may in some cases engage different brain systems (S. Liu et al., 2021).

Finding a correlation with cerebellar activity for CB is particularly interesting, as this region is considered crucial to the control of eye movement. Multiple cerebellar subregions are involved in controlling different aspects of eye movements: Crus I and Crus II for control of smooth pursuit eye movements, lateral cerebellum for control of saccadic eye movements and posterior lobe for integration of sensory information from the visual and vestibular systems to coordinate eye movements (reviewed in Kheradmand & Zee, 2011; Shemesh & Zee, 2019). For CB, we find extensive positive correlations in the posterior cerebellum, potentially suggesting an intact integration of ocular and vestibular information at the cerebellar level, even if lacking a vestibulo-ocular reflex.

We examined the impact of removing the EO-EPI variance on the topography and the causal structure of brain connectivity. We found no difference in the RS networks after removing the EO-EPI signal. This lack of difference indicates that in case of loss of vision from birth, spontaneous eye movements do not strongly mediate connectivity between RS networks. Therefore, connectivity differences in RS networks as shown in previous studies (Bock & Fine, 2014; Guerreiro et al., 2015; Sen et al., 2022), and in our work, cannot be attributed to the difference in the spontaneous eye movements. The fact that seed-based analysis showed a significant relationship between RS activity implies that EO-EPI of CB is still related to cortical activity, but not at the network level. Alternatively, the sample size may restrict the ability to

identify changes at the network level (as supported by the small-N simulation applied to our prior data).

4.1 | Limitations and directions for future research

A limitation of the study is the low statistical power available with only 14 participants. This is an inherent limitation in studies of CB, which (after controlling for multiple comparisons) only identify strong effects. Another limitation is the fact that we did not study in depth potential systematic differences in the connectivity of each eye. As shown in Figure 4, some CB showed no correlation or even negative correlations between the EO-EPI time series of the two eyes. However, these correlations should be treated with caution because Pearson's correlation essentially Z-normalizes each time series, whereas our examination suggested that several of these cases were associated with reduced dynamics in one eye and that even in cases in negative correlations, short epochs of coordinated movements were still observed.

Another limitation is that the study lacked eye tracking data, and so it was not possible to determine whether the EO-EPI data are linked to drifts or abrupt, saccade-like movements. Given the EPI repetition time, it is not possible to determine this information from those data alone.

4.2 | Conclusions

Our findings are the first to show that eye movement activity in CB is systematically linked to patterns of brain activity in both cortical and cerebellar areas. Furthermore, eye movement activity produces whole-brain correlates with a moderate resemblance to activation patterns found for SC, particularly in sensorimotor cortices. At the same time, we document significant differences, including the sign of the correlations with the motor cortex, and the very different frequency characteristics of the EO-EPI data for CB. Our study suggests that oculomotor circuitry is not isolated in the CB but is partially integrated into new neural circuits. The functionality of these eye-linked circuits remains to be understood in future work.

AUTHOR CONTRIBUTIONS

Uri Hasson, Cemal Koba, Emiliano Ricciardi and Olivier Collignon conceived the experiment(s); Uri Hasson and Cemal Koba determined the analysis protocol; Cemal Koba and Alessandro Crimi conducted data analysis; Olivier Collignon contributed neuroimaging data; Uri

Hasson and Cemal Koba drafted the manuscript; all authors reviewed and edited the draft.

ACKNOWLEDGEMENTS

C.K. was supported by the project of the Minister of Science and Higher Education "Support for the activity of Centers of Excellence established in Poland under Horizon 2020" on the basis of the contract number MEiN/2023/DIR/379, and the European Union's Horizon 2020 research and innovation programme under grant agreement No. 857533, and by Sano project carried out within the International Research Agendas programme of the Foundation for Polish Science, co-financed by the European Union under the European Regional Development Fund. U.H. was supported by funding from Italian PNRR project "INNOVA", financed by the Italian Health Ministry.

CONFLICT OF INTEREST STATEMENT

The authors declare no conflict of interest.

PEER REVIEW

The peer review history for this article is available at <https://www.webofscience.com/api/gateway/wos/peer-review/10.1111/ejn.16459>.

DATA AVAILABILITY STATEMENT

The entire analysis code and single-participant fMRI data reporting the per-voxel beta value for the EO-EPI regressor are available at: https://github.com/KobaCemal/EOEPI_for_CB

ORCID

Cemal Koba  <https://orcid.org/0000-0001-7097-1441>

Alessandro Crimi  <https://orcid.org/0000-0001-5397-6363>

Olivier Collignon  <https://orcid.org/0000-0003-1882-3550>

Emiliano Ricciardi  <https://orcid.org/0000-0002-7178-9534>

Uri Hasson  <https://orcid.org/0000-0002-8530-5051>

REFERENCES

- Abraham, A., Pedregosa, F., Eickenberg, M., Gervais, P., Mueller, A., Kossaifi, J., Gramfort, A., Thirion, B., & Varoquaux, G. (2014). Machine learning for neuroimaging with scikit-learn. *Frontiers in Neuroinformatics*, 8(14), 71792. <https://doi.org/10.3389/fninf.2014.00014>
- Allik, J., Rauk, M., & Luuk, A. (1981). Control and sense of eye movement behind closed eyelids. *Perception*, 10(1), 39–51. <https://doi.org/10.1068/p100039>
- Avants, B., Epstein, C., Grossman, M., & Gee, J. (2008). Symmetric diffeomorphic image registration with cross-correlation: Evaluating automated labeling of elderly and neurodegenerative

- brain. *Medical Image Analysis*, 12(1), 26–41. <https://doi.org/10.1016/j.media.2007.06.004>
- Beauchamp, M. S. (2003). Detection of eye movements from fMRI data. *Magnetic Resonance in Medicine: An Official Journal of the International Society for Magnetic Resonance in Medicine*, 49(2), 376–380. <https://doi.org/10.1002/mrm.10345>
- Bernardi, G., Ricciardi, E., Sani, L., Gaglianese, A., Papasogli, A., Ceccarelli, R., Franzoni, F., Galetta, F., Santoro, G., Goebel, R., & Pietrini, P. (2013). How skill expertise shapes the brain functional architecture: An fMRI study of visuo-spatial and motor processing in professional racing-car and naive drivers. *PLoS ONE*, 8(10), e77764. <https://doi.org/10.1371/journal.pone.0077764>
- Bock, A. S., & Fine, I. (2014). Anatomical and functional plasticity in early blind individuals and the mixture of experts architecture. *Frontiers in Human Neuroscience*, 8, 971. <https://doi.org/10.3389/fnhum.2014.00971>
- Brodoehl, S., Witte, O. W., & Klingner, C. M. (2016). Measuring eye states in functional mri. *BMC Neuroscience*, 17(48), 1–10. <https://doi.org/10.1186/s12868-016-0282-7>
- Castaldi, E., Lunghi, C., & Morrone, M. C. (2020). Neuroplasticity in adult human visual cortex. *Neuroscience & Biobehavioral Reviews*, 112, 542–552. <https://doi.org/10.1016/j.neubiorev.2020.02.028>
- Coiner, B., Pan, H., Bennett, M. L., Bodien, Y. G., Iyer, S., O'Neil-Pirozzi, T. M., Leung, L., Giacino, J. T., & Stern, E. (2019). Functional neuroanatomy of the human eye movement network: A review and atlas. *Brain Structure and Function*, 224, 2603–2617. <https://doi.org/10.1007/s00429-019-01932-7>
- Collignon, O., Dormal, G., De Heering, A., Lepore, F., Lewis, T. L., & Maurer, D. (2015). Long-lasting crossmodal cortical reorganization triggered by brief postnatal visual deprivation. *Current Biology*, 25(18), 2379–2383. <https://doi.org/10.1016/j.cub.2015.07.036>
- Cox, R. W. (1996). AFNI: Software for analysis and visualization of functional magnetic resonance neuroimages. *Computers and Biomedical Research*, 29(3), 162–173. <https://doi.org/10.1006/cbmr.1996.0014>
- Desikan, R. S., Ségonne, F., Fischl, B., Quinn, B. T., Dickerson, B. C., Blacker, D., Buckner, R. L., Dale, A. M., Maguire, R. P., Hyman, B. T., Albert, M. S., & Killiany, R. J. (2006). An automated labeling system for subdividing the human cerebral cortex on mri scans into gyral based regions of interest. *NeuroImage*, 31(3), 968–980. <https://doi.org/10.1016/j.neuroimage.2006.01.021>
- Dickey, D. A., & Fuller, W. A. (1979). Distribution of the estimators for autoregressive time series with a unit root. *Journal of the American Statistical Association*, 74(366a), 427–431.
- Diedrichsen, J., Balsters, J. H., Flavell, J., Cussans, E., & Ramnani, N. (2009). A probabilistic mr atlas of the human cerebellum. *NeuroImage*, 46(1), 39–46. <https://doi.org/10.1016/j.neuroimage.2009.01.045>
- Diedrichsen, J., & Zhi, D. (2022, November). A collection of Atlases for the human cerebellum (Version 1.0). https://github.com/DiedrichsenLab/cerebellar_atlases
- Duggento, A., Passamonti, L., Valenza, G., Barbieri, R., Guerrisi, M., & Toschi, N. (2018). Multivariate Granger causality unveils directed parietal to prefrontal cortex connectivity during task-free MRI. *Scientific Reports*, 8(1), 5571. <https://doi.org/10.1038/s41598-018-23996-x>
- Esteban, O., Blair, R., Markiewicz, C. J., Berleant, S. L., Moodie, C., Ma, F., Isik, A. I., Erramuzpe, A., Kent, M., James, D., Goncalves, M., DuPre, E., Sitek, K. R., Gomez, D. E. P., Lurie, D. J., Ye, Z., Poldrack, R. A., & Gorgolewski, K. (2018). Fmriprep. *Software*. <https://doi.org/10.5281/zenodo.852659>
- Esteban, O., Markiewicz, C., Blair, R. W., Moodie, C., Isik, A. I., Erramuzpe Aliaga, A., Kent, J., Goncalves, M., DuPre, E., Snyder, M., Oya, H., Ghosh, S., Wright, J., Durnee, J., Poldrack, R., & Gorgolewski, K. (2018). fMRIPrep: A robust preprocessing pipeline for functional MRI. *Nature Methods*, 16, 111–116. <https://doi.org/10.1038/s41592-018-0235-4>
- Fine, I., & Park, J.-M. (2018). Blindness and human brain plasticity. *Annual Review of Vision Science*, 4, 337–356. <https://doi.org/10.1146/annurev-vision-102016-061241>
- Fonov, V., Evans, A., McKinstry, R., Almlí, C., & Collins, D. (2009). Unbiased nonlinear average age-appropriate brain templates from birth to adulthood. *NeuroImage*, 47(Supplement 1), S102. [https://doi.org/10.1016/S1053-8119\(09\)70884-5](https://doi.org/10.1016/S1053-8119(09)70884-5)
- Frey, M., Nau, M., & Doeller, C. F. (2021). Magnetic resonance-based eye tracking using deep neural networks. *Nature Neuroscience*, 24(12), 1772–1779. <https://doi.org/10.1038/s41593-021-00947-w>
- Glen, D., Reynolds, R., Taylor, P., You, X., Kong, R., Xue, A., Yan, X., & Yeo, B. T. (2021). Improved rois with afni+ suma processing. 27th annual meeting of the Organization for Human Brain Mapping, Poster 1672.
- Gorgolewski, K., Auer, T., Calhoun, V. D., Craddock, R. C., Das, S., Duff, E. P., Flandin, G., Ghosh, S. S., Glatard, T., Halchenko, Y. O., et al. (2016). The brain imaging data structure, a format for organizing and describing outputs of neuroimaging experiments. *Scientific Data*, 3(1), 160044. <https://doi.org/10.1038/sdata.2016.44>
- Gorgolewski, K., Burns, C. D., Madison, C., Clark, D., Halchenko, Y. O., Waskom, M. L., & Ghosh, S. (2011). Nipype: A flexible, lightweight and extensible neuroimaging data processing framework in python. *Frontiers in Neuroinformatics*, 5, 13. <https://doi.org/10.3389/fninf.2011.00013>
- Gorgolewski, K., Esteban, O., Markiewicz, C. J., Ziegler, E., Ellis, D. G., Notter, M. P., Jarecka, D., Johnson, H., Burns, C., Manhães-Savio, A., Hamalainen, C., Yvernault, B., Salo, T., Jordan, K., Goncalves, M., Waskom, M., Clark, D., Wong, J., Loney, F., & Ghosh, S. (2018). Nipype. *Software*. <https://doi.org/10.5281/zenodo.596855>
- Greve, D. N., & Fischl, B. (2009). Accurate and robust brain image alignment using boundary-based registration. *NeuroImage*, 48(1), 63–72. <https://doi.org/10.1016/j.neuroimage.2009.06.060>
- Guerreiro, M. J., Erfort, M. V., Henssler, J., Putzar, L., & Röder, B. (2015). Increased visual cortical thickness in sight-recovery individuals. *Human Brain Mapping*, 36(12), 5265–5274. <https://doi.org/10.1002/hbm.23009>
- Guerreiro, M. J., Linke, M., Lingareddy, S., Kekunnaya, R., & Röder, B. (2021). The effect of congenital blindness on resting-state functional connectivity revisited. *Scientific Reports*, 11(1), 1–14.
- Hölig, C., Guerreiro, M. J., Lingareddy, S., Kekunnaya, R., & Röder, B. (2022). Sight restoration in congenitally blind

- humans does not restore visual brain structure. *Cerebral Cortex*, 33(5), 2152–2161. <https://doi.org/10.1093/cercor/bhac197>
- Jenkinson, M., Bannister, P., Brady, M., & Smith, S. (2002). Improved optimization for the robust and accurate linear registration and motion correction of brain images. *NeuroImage*, 17(2), 825–841. <https://doi.org/10.1006/nimg.2002.1132>
- Jenkinson, M., & Smith, S. (2001). A global optimisation method for robust affine registration of brain images. *Medical Image Analysis*, 5(2), 143–156. [https://doi.org/10.1016/S1361-8415\(01\)00036-6](https://doi.org/10.1016/S1361-8415(01)00036-6)
- Keck, I. R., Fischer, V., Puntonet, C. G., & Lang, E. W. (2009). Eye movement quantification in functional MRI data by spatial independent component analysis. In T. Adali, C. Jutten, J. M. T. Romano, & A. K. Barros (Eds.), *Independent component analysis and signal separation*. ICA 2009. Lecture Notes in Computer Science (Vol. 5441) (pp. 435–442). Springer. https://doi.org/10.1007/978-3-642-00599-2_55
- Kheradmand, A., & Zee, D. (2011). Cerebellum and ocular motor control. *Frontiers in Neurology*, 2, 53. <https://doi.org/10.3389/fneur.2011.00053>
- King, M., Hernandez-Castillo, C. R., Poldrack, R. A., Ivry, R. B., & Diedrichsen, J. (2019). Functional boundaries in the human cerebellum revealed by a multi-domain task battery. *Nature Neuroscience*, 22(8), 1371–1378. <https://doi.org/10.1038/s41593-019-0436-x>
- Koba, C., Notaro, G., Tamm, S., Nilsonne, G., & Hasson, U. (2021). Spontaneous eye movements during eyes-open rest reduce resting-state-network modularity by increasing visual-sensorimotor connectivity. *Network Neuroscience*, 5(2), 451–476. https://doi.org/10.1162/netn_a_00186
- Kompf, D., & Piper, H.-F. (1987). Eye movements and vestibulo-ocular reflex in the blind. *Journal of Neurology*, 234(5), 337–341. <https://doi.org/10.1007/bf00314291>
- Lanczos, C. (1964). Evaluation of noisy data. *Journal of the Society for Industrial and Applied Mathematics Series B Numerical Analysis*, 1(1), 76–85. <https://doi.org/10.1137/0701007>
- Leigh, R. J., & Zee, D. S. (1980). Eye movements of the blind. *Investigative Ophthalmology & Visual Science*, 19(3), 328–331.
- Liu, S., Zhao, B., Shi, C., Ma, X., Sabel, B. A., Chen, X., & Tao, L. (2021). Ocular dominance and functional asymmetry in visual attention networks. *Investigative Ophthalmology & Visual Science*, 62(4), 9–9. <https://doi.org/10.1167/iovs.62.4.9>
- Liu, Y., Yu, C., Liang, M., Li, J., Tian, L., Zhou, Y., Qin, W., Li, K., & Jiang, T. (2007). Whole brain functional connectivity in the early blind. *Brain*, 130(8), 2085–2096. <https://doi.org/10.1093/brain/awm121>
- MATLAB version 9.10.0.1613233 (R2021a). (2021). *The Mathworks*. Inc.
- Nilsonne, G., Tamm, S., D'Onofrio, P., Thuné, H. Å., Schwarz, J., Lavebratt, C., Liu, J. J., Månsson, K. N., Sundelin, T., Axelsson, J., Petrovic, P., Fransson, P., Kecklund, G., Fischer, H., Lekander, M., & Åkerstedt, T. (2016). A multi-modal brain imaging dataset on sleep deprivation in young and old humans, 1–27. <https://openarchive.ki.se/xmlui/handle/10616/45181>
- Pelland, M., Orban, P., Dansereau, C., Lepore, F., Bellec, P., & Collignon, O. (2017). State-dependent modulation of functional connectivity in early blind individuals. *NeuroImage*, 147, 532–541. <https://doi.org/10.1016/j.neuroimage.2016.12.053>
- Pouget, P. (2015). The cortex is in overall control of ‘voluntary’ eye movement. *Eye*, 29(2), 241–245. <https://doi.org/10.1038/eye.2014.284>
- Power, J. D., Mitra, A., Laumann, T. O., Snyder, A. Z., Schlaggar, B. L., & Petersen, S. E. (2014). Methods to detect, characterize, and remove motion artifact in resting state fMRI. *NeuroImage*, 84(Supplement C), 320–341. <https://doi.org/10.1016/j.neuroimage.2013.08.048>
- Rolls, E. T., Joliot, M., & Tzourio-Mazoyer, N. (2015). Implementation of a new parcellation of the orbitofrontal cortex in the automated anatomical labeling atlas. *NeuroImage*, 122, 1–5. <https://doi.org/10.1016/j.neuroimage.2015.07.075>
- Rorden, C., & Brett, M. (2000). Stereotaxic display of brain lesions. *Behavioural Neurology*, 12(4), 191–200. <https://doi.org/10.1155/2000/421719>
- Rorden, C., Karnath, H. O., & Bonilha, L. (2007). Improving lesion-symptom mapping. *Journal of Cognitive Neuroscience*, 19, 1081–1088. <https://doi.org/10.1162/jocn.2007.19.7.1081>
- Rubinov, M., & Sporns, O. (2010). Complex network measures of brain connectivity: Uses and interpretations. *NeuroImage*, 52, 1059–1069. <https://doi.org/10.1016/j.neuroimage.2009.10.003>
- Saenz, M., Lewis, L. B., Huth, A. G., Fine, I., & Koch, C. (2008). Visual motion area mt+/v5 responds to auditory motion in human sight-recovery subjects. *Journal of Neuroscience*, 28(20), 5141–5148. <https://doi.org/10.1523/JNEUROSCI.0803-08.2008>
- Schaefer, A., Kong, R., Gordon, E. M., Laumann, T. O., Zuo, X.-N., Holmes, A. J., Eickhoff, S. B., & Yeo, B. T. T. (2018). Local-global parcellation of the human cerebral cortex from intrinsic functional connectivity MRI. *Cerebral Cortex*, 28, 3095–3114. <https://doi.org/10.1093/cercor/bhx179>
- Schöpf, V., Schlegl, T., Jakab, A., Kasprian, G., Woitek, R., Prayer, D., & Langs, G. (2014). The relationship between eye movement and vision develops before birth. *Frontiers in Human Neuroscience*, 8, 775. <https://doi.org/10.3389/fnhum.2014.00775>
- Seabold, S., & Perktold, J. (2010). Statsmodels: Econometric and statistical modeling with python. *9TH PYTHON IN SCIENCE CONFERENCE*, 57–61.
- Sen, S., Khalsa, N. N., Tong, N., Ovadia-Caro, S., Wang, X., Bi, Y., & Striem-Amit, E. (2022). The role of visual experience in individual differences of brain connectivity. *Journal of Neuroscience*, 42(25), 5070–5084. <https://doi.org/10.1523/JNEUROSCI.1700-21.2022>
- Shehzad, Z., Kelly, A. C., Reiss, P. T., Gee, D. G., Gotimer, K., Uddin, L. Q., Lee, S. H., Margulies, D. S., Roy, A. K., Biswal, B. B., et al. (2009). The resting brain: Unconstrained yet reliable. *Cerebral Cortex*, 19(10), 2209–2229. <https://doi.org/10.1093/cercor/bhn256>
- Shemesh, A. A., & Zee, D. S. (2019). Eye movement disorders and the cerebellum. *Journal of Clinical Neurophysiology: Official Publication of the American Electroencephalographic Society*, 36(6), 405–414. <https://doi.org/10.1097/WNP.0000000000000579>
- Son, J., Ai, L., Lim, R., Xu, T., Colcombe, S., Franco, A. R., Cloud, J., LaConte, S., Lisinski, J., Klein, A., Craddock, R. C., & Milham, M. (2020). Evaluating fMRI-based estimation of eye gaze during naturalistic viewing. *Cerebral Cortex*, 30(3), 1171–1184. <https://doi.org/10.1093/cercor/bhz157>

- Tustison, N. J., Avants, B. B., Cook, P. A., Zheng, Y., Egan, A., Yushkevich, P. A., & Gee, J. C. (2010). N4itk: Improved n3 bias correction. *IEEE Transactions on Medical Imaging*, 29(6), 1310–1320. <https://doi.org/10.1109/TMI.2010.2046908>
- van der Meer, J. N., Pampel, A., Van Someren, E. J., Ramautar, J. R., van der Werf, Y. D., Gomez-Herrero, G., Lepsien, J., Hellrung, L., Hinrichs, H., Möller, H. E., et al. (2016). Carbon-wire loop based artifact correction outperforms post processing EEG/fMRI corrections—A validation of a real-time simultaneous EEG/fMRI correction method. *NeuroImage*, 125, 880–894. <https://doi.org/10.1016/j.neuroimage.2015.10.064>
- Van Rossum, G., & Drake, F. L. (2009). *Python 3 reference manual*. CreateSpace.
- Voss, P. (2019). Brain (re) organization following visual loss. *Wiley Interdisciplinary Reviews: Cognitive Science*, 10(1), e1468. <https://doi.org/10.1002/wcs.1468>
- Winkler, A. M., Ridgway, G. R., Webster, M. A., Smith, S. M., & Nichols, T. E. (2014). Permutation inference for the general linear model. *NeuroImage*, 92, 381–397. <https://doi.org/10.1016/j.neuroimage.2014.01.060>
- Xia, M., Wang, J., & He, Y. (2013). Brainnet viewer: A network visualization tool for human brain connectomics. *PLoS ONE*, 8(7), e68910. <https://doi.org/10.1371/journal.pone.0068910>
- Yarkoni, T., Poldrack, R. A., Nichols, T. E., Van Essen, D. C., & Wager, T. D. (2011). Large-scale automated synthesis of human functional neuroimaging data. *Nature Methods*, 8, 665–670. <https://doi.org/10.1038/nmeth.1635>
- Zalesky, A., Fornito, A., & Bullmore, E. T. (2010). Network-based statistic: Identifying differences in brain networks. *NeuroImage*, 53(4), 1197–1207. <https://doi.org/10.1016/j.neuroimage.2010.06.041>
- Zhang, Y., Brady, M., & Smith, S. (2001). Segmentation of brain MR images through a hidden Markov random field model and the expectation-maximization algorithm. *IEEE Transactions on Medical Imaging*, 20(1), 45–57. <https://doi.org/10.1109/42.906424>

SUPPORTING INFORMATION

Additional supporting information can be found online in the Supporting Information section at the end of this article.

How to cite this article: Koba, C., Crimi, A., Collignon, O., Ricciardi, E., & Hasson, U. (2024). Neural networks associated with eye movements in congenital blindness. *European Journal of Neuroscience*, 60(4), 4624–4638. <https://doi.org/10.1111/ejn.16459>